


Corrosion Resistant CrN_x Nanolayers Obtained by Low Temperature Ion Nitriding of Hard Chromium Coated AISI 1045 Steel

J.A. Díaz-Elizondo^a, J.C. Díaz-Guillén^b, N.A. Rodríguez-Rosales^a, E.E. Granda Gutiérrez^c,
G. Ochoa-Hernández^d, S. Mancillas-Salas^e, J.A. Díaz Guillén^{a*} 

^aTecnológico Nacional de México, IT Saltillo, 25280, Saltillo, México.

^bCONACYT, Corporación Mexicana de Investigación en Materiales, 25290, Saltillo, México.

^cUniversidad Autónoma del Estado de México, 50400, Atlacomulco, México.

^dUniversidad Virtual del Estado de Michoacán, 58147, Morelia, México.

^eCentro de Investigación y de Estudios Avanzados del IPN, Unidad Saltillo, 25900, Ramos Arizpe, México.

Received: January 12, 2021; Revised: April 15, 2021; Accepted: May 18, 2021

Chromium nitrides Cr_xN have attracted research interest due to their excellent wear and corrosion properties when are deposited on steels. Nevertheless, due to the considerable difference between Cr_xN and steel expansion coefficients, microcracks and delamination are still persistent problems. In this regard, this research addressed the generation of CrN_x nanolayers, through an ion nitriding process, carried out on hard chromium coated AISI 1045 steel. The effect of nitriding temperature (500°C-550°C) and nitrogen content in plasma (25, 50, and 75%) on corrosion performance and layer characteristics were studied. Grazing Incidence X-ray Diffraction analysis revealed that modified surfaces are composed of nanolayers, constituted by a mixture of CrN, Cr₂N, Cr, and Fe₄N. Rietveld quantification shows that the fraction of chromium nitrides in the region analyzed increased with increasing both temperature and nitrogen content in plasma, resulting CrN as the predominant phase for all evaluated conditions. The electrochemical behavior of the modified nanolayers was studied by potentiodynamic polarization technique, revealing an enhancement in corrosion performance of chromium coated 1045 steel by the nitriding treatment, showing a corrosion current density 10 times lower than the untreated sample and more positive corrosion potentials for the nitrided samples concerning chromium coated 1045 steel.

Keywords: Ion nitriding, AISI 1045, Chromium nitrides, Hard chromium.

1. Introduction

Specific properties such as high corrosion resistance and excellent wear performance have been required through time in metallic components used in food, metalworking, and electronics industry. In the last decades the application of hard chromium coatings on the steel or alloys components has been a widely alternative to improve corrosion and wear resistance of components as engine parts or cutting tools¹. Although the development and extensive use of hard chromium coating processes, these coatings are still accompanied by microcracks and delamination defects, causing a decrease in the lifespan of the coating since corrosive reagents can diffuse into the substrate through these defects².

Various studies have demonstrated that transition metal nitrides are excellent candidates to replace or modify the well-known hard chromium coatings. These interstitial compounds can be obtained by different superficial modification techniques, including thermochemical treatments such as gas nitriding and physical vapor deposition³⁻⁶, cathodic evaporation^{7,8} and magnetron sputtering⁹⁻¹¹, to mention a few. Chromium nitrides (Cr_xN) are transition metal nitrides that have been of great interest in the last years due to

their high resistance to wear and corrosion. This type of compounds have gained interest in several applications, such as cutting tools, injection molding and bipolar plates for Low-Temperature Fuel Cells¹². Nevertheless, due to their important differences in thermal expansion coefficients, there are some problems during synthesizing this type of interstitial compounds directly on the steel surface^{13,14}, which generate microcracks or even delamination of the coating. For solving this problem, researchers have deposited a hard chromium coating on the surface of the steel since it has an intermediate thermal expansion coefficient between Cr_xN and the steel^{15,16}. Although there is extensive information related to the structure and phases of Cr_xN (including effects on the corrosion resistance) applied by cathodic evaporation, magnetron and high-temperature gas nitriding^{17,18}, there is still scarce current information involving the same phases synthesized by the ion nitriding process, a technique that offers high control of parameters, low temperature and relative short processing time¹³.

Wierzchon et al.¹⁹ investigated the formation of chromium nitrides, oxynitrides and oxide by ion nitriding, in an Armco iron and AISI 1045 steel, which were electrochemically coated with hard chromium, reporting that the corrosion

*e-mail: jadiaz@itsaltillo.edu.mx

resistance of these layers in the coating of hard chromium is elevated and can even be improved by modifying the process variables such as temperature and partial pressure of nitrogen. On the other hand, Menthe and Rie² reported a process of plasma nitriding on a steel with hard chromium coating at 560°C and 700°C, to different processing times (5 to 20 h), finding the formation of a chromium nitrides mixture (CrN, Cr₂N and Cr) in the nitrided region, showing a significant improvement in corrosion resistance. Sarraf et al.²⁰ also reported the ion nitriding technique to repair microcracks in a hard chrome surface, revealing the formation of different CrN and Cr₂N phases after the nitriding process. The results showed an improvement in corrosion resistance, in 3.5 wt% NaCl solution. Likewise, Aghajani et al.²¹ investigated the effect of plasma nitriding on H11 steel coated with hard chromium at ion nitriding temperature of 550°C for different process times, obtaining a mixture of CrN, Cr₂N, Cr, Fe₂₋₃N and Fe₄N phases in the modified zone. As well as Taktak et al.²² who studied the ionic nitriding process in AISI 52100 and 8620 steels coated with hard chromium, using different gas mixtures, revealing an improvement in the wear properties due to the formation of CrN and Cr₂N.

Therefore, this research is based on the formation of nanolayers composed mainly of corrosion-resistant Cr_xN; it is also intended to show that the corrosion resistance of Cr_xN can be efficient at a short time and low temperature at the nitriding process. These treatment conditions could result in a more efficient and profitable nitriding process with a high possibility for industrial applications (e.g. fuel cells bipolar plates or diluting magnetic semiconductors). On the other hand, the effect of nitrogen content in plasma on the formation of different types of Cr_xN is studied, as well as its influence on corrosion resistance of coated steel.

2. Experimental Procedure

The CrN_x-type ceramic coatings were developed on commercial 10 x 10 x 5 mm³ coupons of AISI (American Iron and Steel Institute)-1045 steel, which were previously coated with a layer of electrolytic hard chromium with ~1.5 μm in thickness. The microstructure of base 1045 steel consists mainly of ferrite and perlite and its weight percentage chemical composition, determined by optical emission spectroscopy (PMI MASTER PRO, Oxford Instruments), was: C 0.49, Si 0.18, Mn 0.62, Cr 0.06, Mo 0.03, Ni 0.04, P 0.014, S 0.04, balance Fe.

The surface modification process was carried out in a 42 L laboratory chamber during 3 h, using a DC glow-discharge in a gas mixture of N₂/H₂ at 266 Pa, at potential of ~580 V, at constant current density of 1.5 mA/cm². The temperature control was carried out through a closed circuit using a PID controller, coupled with a type K thermocouple in direct contact with sample. Mass flow controllers were used to modifying the N₂/H₂ rate in the plasma. After treatment, samples were cooled to room temperature inside the vacuum chamber with an argon inert atmosphere. Conditions of nitriding for different samples and their identification are shown in Table 1.

Table 1. Identification and processing conditions of plasma nitrided samples.

Samples ID	Temperature (°C)	N ₂ in plasma (%)
S1	500	25
S2		50
S3		75
S4	550	25
S5		50
S6		75

Surface and cross-section morphologies of the nitrided samples were analyzed by Scanning Electron Microscopy (SEM) (TESCAN MIRA 3). Nitrogen semi-quantitative profiles were determined by X-ray energy dispersion spectrometry (EDS) coupled to SEM. As corrosion resistance is related to the crystalline phases present on the surface, phases on nitrided samples were identified using Grazing Incidence X-ray Diffraction (GIXRD) with incidence angles set at 0.5 and 5°. This analysis was carried out on an Empyrean Analytical X-ray diffractometer in a 2 theta range from 35 to 55°, with a scan speed of 17s/step with increments of 0.018°, using Cu Kα radiation at 45 kV and 40 mA. In order to quantify the present phases in the modified surfaces, Rietveld refinement of XRD patterns (0.5 incidence angle) was performed for all nitrided samples.

The penetration depth of the X-ray during XRD analysis, was estimated by Equation 1²³, within the region of the most intense peaks in the patterns, assuming a location at 2θ angles of 43.65° for the main reflection of CrN and 44.58° for the main reflection of Cr-α,

$$d = \left[\mu \left(\frac{1}{\sin \alpha} + \frac{1}{\sin(2\theta - \alpha)} \right) \right]^{-1} \quad (1)$$

where α represents the incidence angle and μ is the linear absorption coefficient. To calculate μ, the mass absorption coefficient (μ/ρ), which depends only of the composition, should be multiplied by the material density, ρ.

Mass absorption coefficients were consulted from the literature²³ and the depth analysis was considered as the depth into the material measured along the surface normal where the intensity of X-ray falls to 1/e of its value at the surface. Likewise, the density of nitrided layers was estimated, considering the mixture of phases (CrN, Cr₂N, Fe₄N, and Cr) determined by Rietveld analysis for each different nitriding treatments.

The corrosion resistance was evaluated by the potentiodynamic method using a potentiostatic galvanostatic Gamry 1000A interface equipment. An experimental arrangement of three electrodes was used with platinum as counter electrode, saturated calomel (SEC) as reference electrode, and nitrided sample as the working electrode. Nitrided samples were immersed in 0.5 M H₂SO₄ solution at room temperature, and the scanning potential was set in a range of -500 to 1200 mV, setting scanning rate at 1 mV/s and stabilizing time of 600 s.

3. Result and Discussion

3.1. Surface and cross morphology

SEM surface morphology of Cr- α coated AISI 1045 is shown in Figure 1. A smooth surface, with an extensive

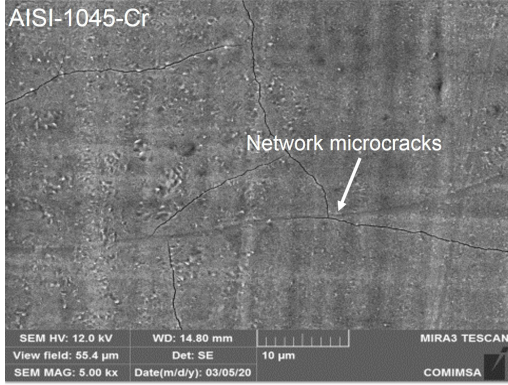


Figure 1. SEM surface picture of AISI1045-Cr.

microcracks network throughout whole the surface of the sample can be observed. This morphology is characteristic of this kind of coatings, due to tensile stress generated during electroplating²⁴.

Surface morphologies of nitrided samples are shown in Figure 2. Ion nitriding treatment at 500°C with different nitrogen contents in plasma (Figures 2 a, b, and c), does not considerably modify the surface morphologies, but it can be appreciated small precipitates on the surfaces and no presence of microcracks. The sealing of the microcracks is due to the unavoidable increase in volume that develops when the Cr_xN is formed, which provides a net volume increase of approximately 45%, causing an expansion of the chromium coating near the surface²⁴.

As the ion nitriding temperature increases from 500 to 550°C, a higher density of precipitates is observed for all nitrogen contents (Figures 2 d, e, and f). The sizes of these irregular shape precipitates are in the range of 1 μ m; and it can be observed how the largest particles are formed by agglomeration mechanisms. In agreement with Shayan *et al.*²⁰, who formed Cr_xN and Fe₄N on tools steel by traditional ion

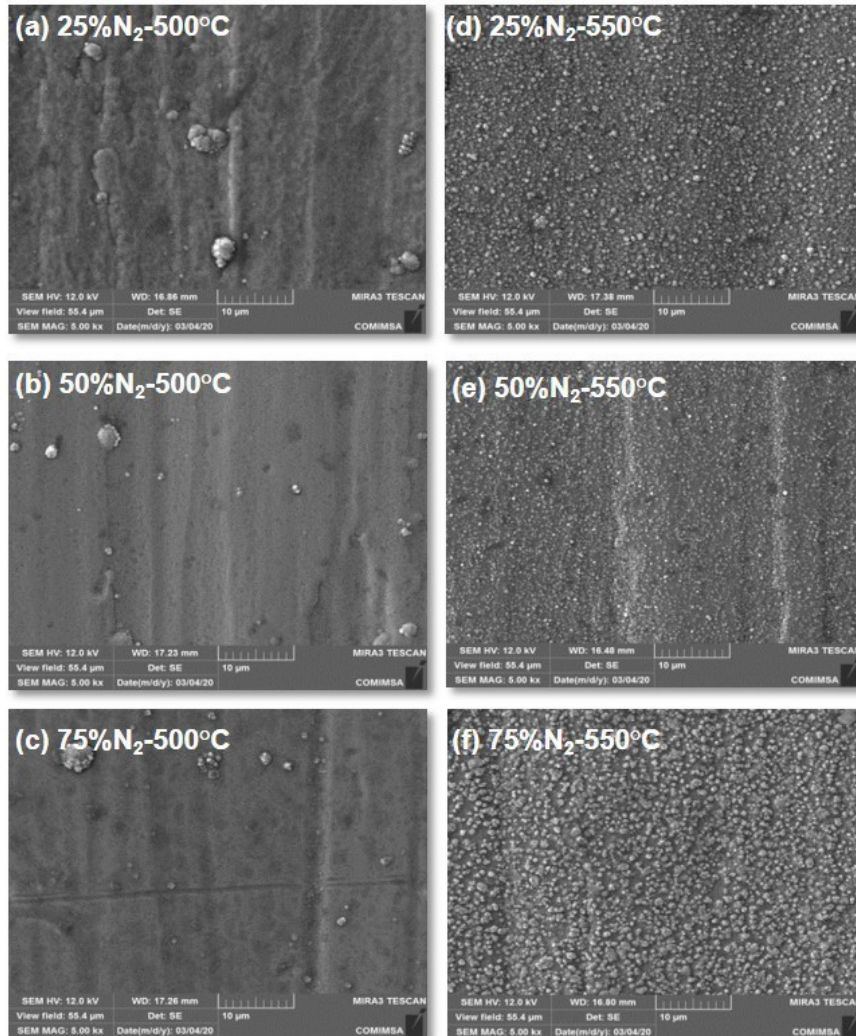


Figure 2. SEM surface pictures of nitrided samples.

nitriding and active screen plasma nitriding, the development of this morphology can be attributed to the effect of cathode sputtering that commonly occurs in the ion nitriding processes.

Figure 3 presents a SEM cross-section micrograph of the sample nitrided at 550°C with 75% of nitrogen in plasma, the hard chromium coating and the nitride nanolayer can be observed. Nitrogen content is also shown for all nitrided samples until a depth of 900 nm, determined by point analysis using EDS. The depths analyzed in the nitrided layers were 0, 500 and 900 nm and an average of 5 microanalysis was recorded for each depth. EDS point analysis reveals a nitrogen profile in nitrided layers, showing a decrease in nitrogen content as depth increases for all treatments.

The samples treated at 550°C present a higher nitrogen content for the different depths analyzed in the nitrided layers, compared to the samples treated at 500°C, which indicates a greater nitrogen absorption at higher temperatures, suggesting an increase in the depth of chromium nitride. This behavior had also been observed by Ajikumar *et al.*²⁵, detecting a greater diffusion of nitrogen for temperatures above 700°C.

The Cr-N binary system provides information on the possible chromium nitride phases that can be obtained by manipulating the temperature and the nitrogen content. In this sense, it can be mentioned that the nitrided layers at

500°C can be shaped by a mixture of Cr and Cr₂N phases in the outermost part of the layer, followed by an expanded structure of chromium with nitrogen. Meanwhile, for the samples treated to 550°C, the layers could be composed of a mixture of Cr₂N and CrN phases up to a depth of 500 nm, according to the nitrogen content obtained in the point EDS analysis for the different treatments.

The formation of Cr_xN on the hard chromium layer in ion and gaseous nitriding processes is controlled by the development of its own diffusion phenomena that depends on chemical kinetics. Buijnsters *et al.*²⁶ reported that the formation of chromium nitride can be explained by the interstitial diffusion of atomic nitrogen in the Cr- α matrix until it reaches saturation of 33% of atomic nitrogen, then a layer of the hexagonal Cr₂N phase begins growing parallelly to the direction of diffusion of nitrogen. As the concentration of nitrogen is higher in the outermost part of the layer due to constant nitrogen bombardment, the cubic CrN phase will begin growing on the surface of the hexagonal phase until a CrN monolayer is obtained.

3.2. Phases structure

Grazing incidence XRD analysis were carried in order to determinate crystalline phases at different depths. Table 2 shows X-ray penetration depth (region from which

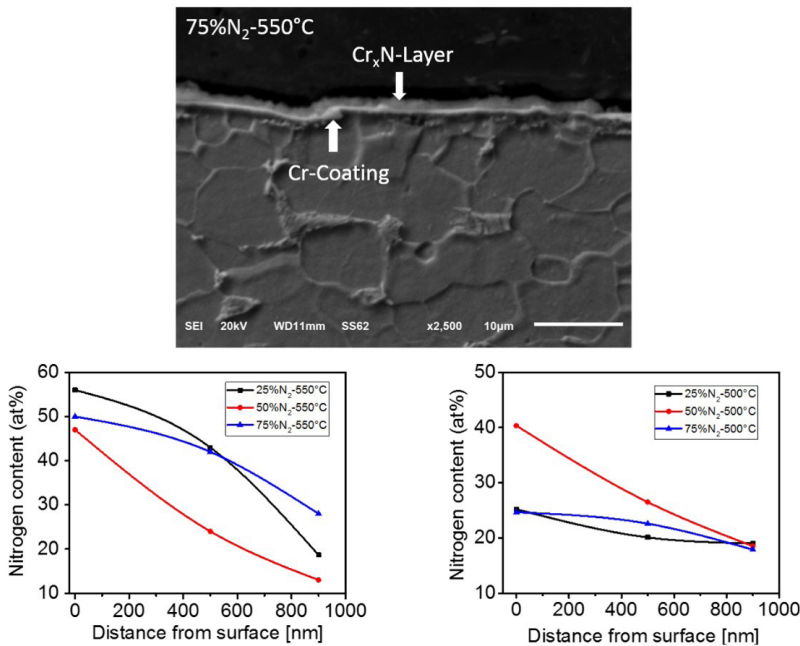


Figure 3. Cross-section SEM micrograph of sample nitrided (S6) and composition profiles for nitrogen of the cross-section in the nitrided layers.

Table 2. X-ray depth in nitrided layers at different angles of incidence

ID sample	S1	S2	S3	S4	S5	S6
ρ (g/cm ³)	7.04	6.99	6.97	6.70	6.82	6.69
μ (cm ⁻¹)	1677	1738	1730	1511	1672	1545
Angle of incidence	500°C		550°C		550°C	
2θ	Depth (nm)		Depth (nm)		Depth (nm)	
0.5°	44.58	51.39	49.64	49.8	57.01	51.52
0.5°	43.68	51.38	49.55	49.79	56.9	51.51
5°	44.58	457.17	440.91	443.03	507.21	458.33
5°	43.68	456.07	439.85	441.96	505.99	457.22

the information is obtained), as well as the values of density and mass absorption coefficient used to determinate them. Main reflections for Cr- α and CrN, located at 44.58° and 43.68° 2 θ angle respectively, were considered for penetration depth compute. In a general way, it can be appreciated that XRD information is obtained from a depth close to 50 nm for 0.5° incidence angle and about from 500 nm in depth for 5° incidence angle.

Figure 4 shows the XRD patterns obtained with an incidence angle of 0.5° for all treatments (information from approximately 50 nm in depth). It can be seen that after applying the ion nitriding treatment at 500°C and 550°C with different nitrogen contents in plasma, a mixture of phases is formed on the modified surface, which is mainly constituted by chromium nitrides (CrN and Cr₂N), in addition to the phases of Fe₄N and metallic Cr- α . These patterns are compared to JCPDS cards 04-003-5919, 04-014-1025, 00-064-0134, and 04-003-5597 as reference.

The treatment at 500°C with nitrogen content of 25% gives place to a mixture of CrN and Cr₂N phases with main reflection at 2 θ positions of 37.5° and 42.7° respectively. The increasing of the plasma nitrogen concentration to 50% and 75% led the presence of a new peak at 43.6°, corresponding to the CrN phase. For a nitriding temperature of 550°C, an increase in the intensities of CrN and Cr₂N phases in the different orientations is observed, as well as a new peak at 40.2° related to Cr₂N phase. The here reported phases are in accordance with the Cr-N phase diagram²⁷.

On the other hand, the reflection corresponding to metallic Cr- α is observed for all nitrided samples, which marks an incomplete transformation towards the different types of chromium nitrides²⁸. This effect could be related to the slow diffusion of atomic nitrogen in chromium nitrides. The nitrogen diffusion is affected by the high compression stresses developed during transformation of chromium nitrides since both phases generate a contribution of expansions, which are preferentially induced in Cr grains. Resulting in reduced kinetics for the transformations of Cr- α in chromium nitrides^{25,26}.

The presence of Fe₄N reflections in 0.5° incidence angle GIXRD patterns for all nitriding samples could be explained by the sputtering phenomenon occurring on the fixtures of the nitriding system (cathode), which has been reported in thermochemical treatments assisted by plasma²⁰. The sputtering intensity is a function of nitriding temperature as well as the plasma composition (N₂/H₂ rate) so, variations in the intensity of Fe₄N reflections can be appreciated in 0.5° GIXRD patterns.

Figure 5 shows the GIXRD patterns obtained using an incidence angle of 5° (information from approximately 500 nm in depth). In this case, the reflections corresponding to Cr_xN are absent for a nitriding temperature of 500°C regardless of nitrogen content in plasma. The phase Cr- α was identified for these conditions. At 550°C, CrN and Cr₂N are evidenced in positions 2 θ of 37.3° and 43.7° for the CrN, and 40.2° and 42.6° for the Cr₂N, which can be an indicative that modified layers at this temperature have a thickness of at least 500 nm. Likewise, a slight shift of the Cr- α reflection towards lower 2 θ angles can be observed for all nitriding conditions and both GIXRD evaluated conditions. This effect could be

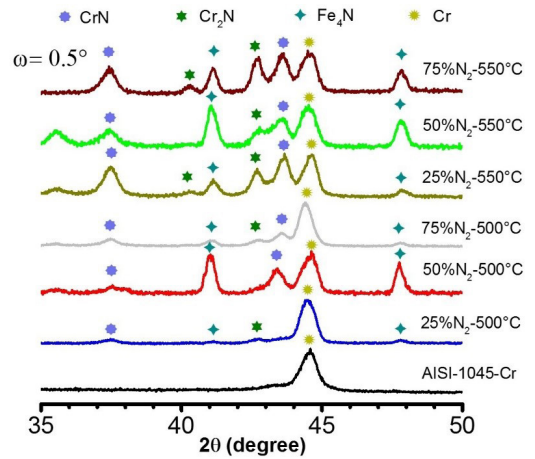


Figure 4. GIXRD patterns at an incidence angle of 0.5° for Cr coated 1045 steel and nitrided samples.

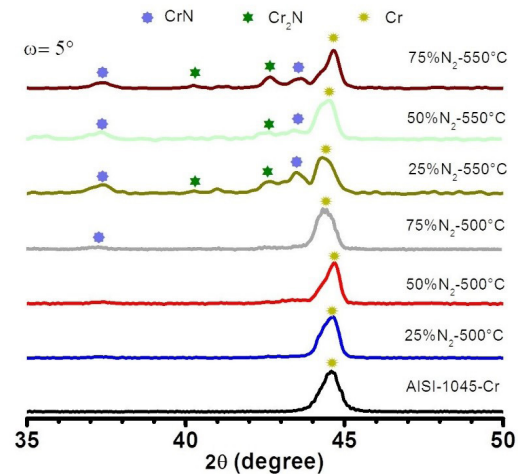


Figure 5. GIXRD patterns at an incidence angle of 5° for Cr coated 1045 steel and nitrided samples.

associated with the insertion of atomic nitrogen in interstitial position of the Cr- α crystalline structure, producing a slight expansion and an increase in lattice parameter^{27,29}.

In Figure 5 it is also appreciated the disappearance of Fe₄N reflections, reinforcing the claim that this phase is only present on the top surface of the nitrided layers, which is attributed to cathodic sputtering phenomenon.

3.3. Phases quantification by Rietveld method

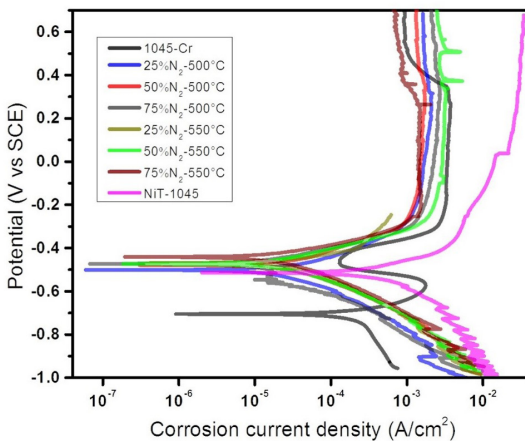
Table 3 shows the phases quantification, at 50 nm in depth, obtained by the Rietveld method for nitrided layers. Phase's quantification reveals an increase in the total content of Cr_xN as a result of the increase in the nitriding temperature. A greater nitriding potential (greater amount of N⁺ cations in the plasma) is expected at higher temperature as well as an increase in the nitrogen diffusion rate and consequently in the synthesized Cr_xN volume. The real fraction of Cr_xN in nitrided layers could be even higher than that presented in Table 3, based on the fact that presented quantification includes Fe₄N phase, which is located only on the most superficial part of the nitrided layer.

Table 3. Rietveld Phases quantification in nitrated layers at a depth of 50 nm

Sample ID	N ₂ in plasma (%)	Temperature (°C)	Cr (%)	CrN (%)	Cr ₂ N (%)	Fe ₄ N (%)
S1	25	500	72.4	15.4	10.5	2.2
S2	50		29.4	36.5	0.7	33.4
S3	75		55.7	26.8	10.1	7.4
S4	25	550	23.3	50.1	18.4	8.2
S5	50		26.0	23.1	24.5	26.4
S6	75		22.4	41.1	21.1	15.4

Table 4. Electrochemical parameters of nitrated samples and base material.

Sample	E _{corr} (mV)	i _{corr} (μA/cm ²)	R _p (Ωcm ²)	Pi(%)
1045-Cr	-707	74.55	144.05	---
S1	-511	12.93	933.48	82.65
S2	-484	15.86	1060.61	78.7
S3	-485	7.11	2453.99	90.46
S4	-472	13.55	1117.69	81.82
S5	-477	12.59	1310.40	83.1
S6	-444	10.51	1328.80	85.9
1045-Nit	-520	708.9	0.637	---

**Figure 6.** Potentiodynamic polarization curves of nitrated samples under different conditions.

On the other hand, it is observed a greater fraction towards the CrN phase with the increase of the nitrogen flow and the nitriding temperature, these results are in good agreement with that reported by Taguchi and Kurihara.³⁰ They evidenced the formation of CrN and Cr₂N at temperatures range of 700°C to 1100°C with a higher selectivity towards CrN, which increases at higher nitrogen concentration or processing time as follows:



3.4. Electrochemical corrosion performance

Figure 6 shows the potentiodynamic polarization curves for nitrated samples at different conditions, as well as the curves for both; base material (1045-Cr) and nitrated 1045 steel.

For all evaluated samples, potentiodynamic polarization curves show a clear definition of the active-passive zone, which allows determining the corrosion rates for each treatment. The nitrated hard chromium layers present more positive values of corrosion potential than base metal and even than only nitrated 1045 steel, indicating a higher thermodynamic resistance to the initiation and evolution of corrosion phenomena. Likewise, a displacement to the left of the curves obtained for nitrated samples is also experienced in reference to the nitrated 1045 steel and the base material, which indicates a lower corrosion rate through a decrease of the corrosion current density. These results reveal that corrosion current densities for the nitrated layers are 10 times reduced regarding the base material.

Table 4 shows the values of corrosion current densities, which let to establish that the different nitrogen contents in plasma and the temperatures used during nitriding do not generate a significant change on them, since all systems have a composite nanolayer of CrN and Cr₂N with a higher fraction of the CrN phase. These results are in good agreement with that reported by Taguchi and Kurihara,³⁰ who studied the formation of a double structure with a phases mixture of CrN and Cr₂N, which improved the corrosion resistance. They also found that a higher fraction of CrN improved the corrosion resistance. The protective efficacy (Pi) of the layers of CrN and Cr₂N, determined using Equation 3³¹ is also presented in Table 4,

$$Pi(\%) = \left(1 - \frac{i_{corr}}{i_{corr}^0} \right) \times 100 \quad (3)$$

where i_{corr}^0 and i_{corr} are the corrosion current densities of the base material and nitrated samples respectively. The protective efficiency of the nanolayers was in an approximated range from 78 to 90%. This result supports the claim that nanolayers composed of CrN and Cr₂N represent an effective means of improving corrosion resistance. In general, transition metal nitrides are inert to chemical attack due to their relatively higher position in the electrochemical series³². In agreement with Wierzchon et al.¹⁹ the corrosion resistance can be explained by the formation of a fine-grained homogeneous nanostructure of chromium nitrides (CrN and Cr₂N), which acts as a barrier and prevents diffusion of the electrolyte to the substrate.

Figure 7 reveals the corroded surface morphologies (SEM) of base material, nitrated steel, and as reference, the samples nitrated at 500°C and 550°C with 75% of nitrogen. EDS analysis confirms that the layer hard chromium of base material was dissolved during the corrosion test

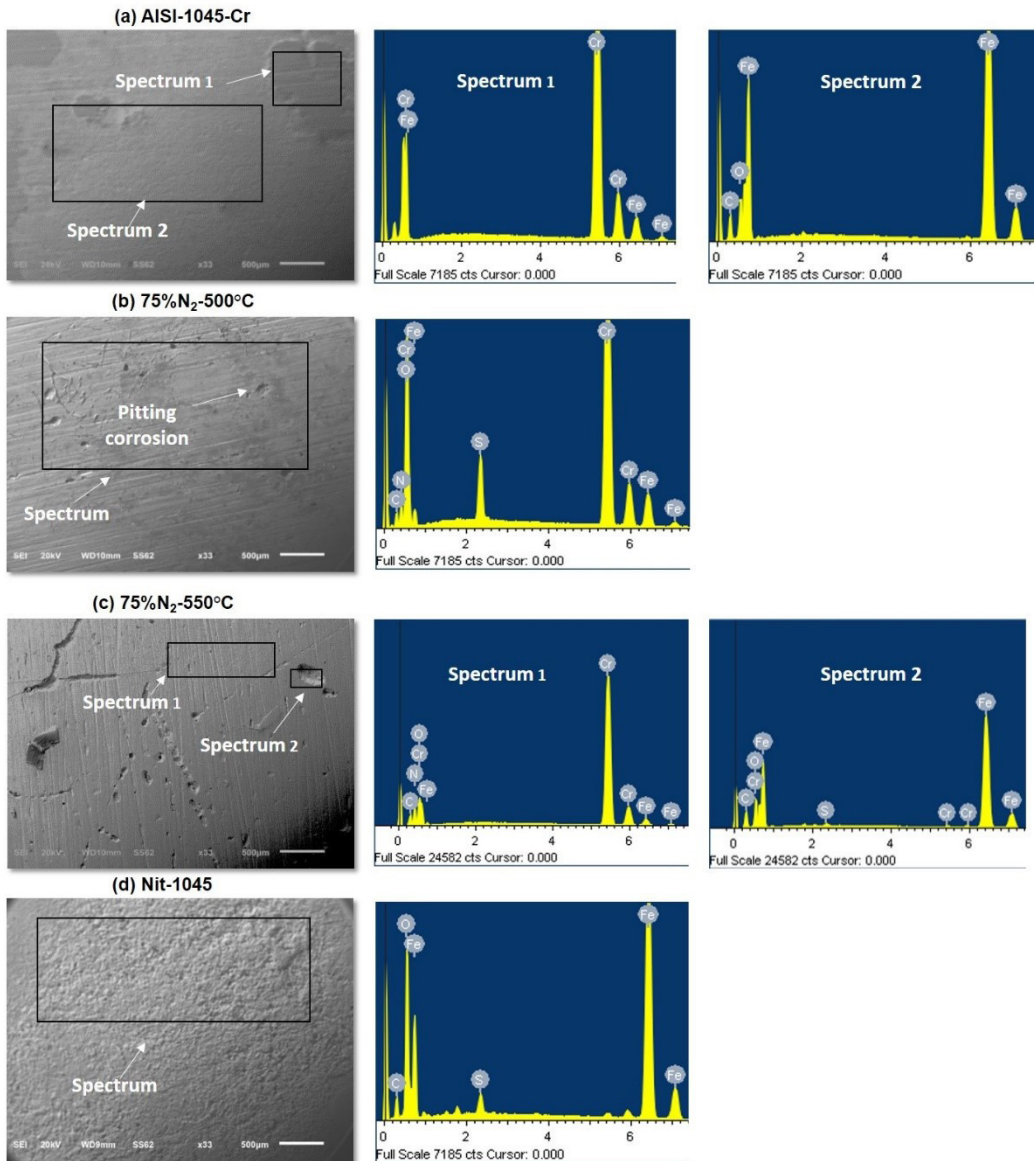


Figure 7. SEM micrographs and EDS spectra obtained for base materials and corroded surfaces of the different ion nitriding treatments.

(see Figure 7a), due to diffusion of the electrolyte through local defects, generating a galvanic couple between the hard chromium coating and the substrate. The corroded surface morphologies of the nitrided samples (Figures 7b and c), show a significant improvement because they do not present severe corrosion after the corrosion test, however small areas with localized corrosion can be observed. Pitting corrosion is also observed in the potentiodynamic polarization test in a potential range of 0.2 to 0.4 V. This performance could be associated with an incomplete sealing of the microcracks and the presence of new local defects in the ceramic nanolayers of Cr_xN. It is known that Cr_xN ceramic coatings present local defects such as microcracks and porosity, which act as channels to transport corrosive agents and generate localized corrosion^{32,33}. Nonetheless, the effect of these new defects is considerably less since the corrosion performance is significantly improved. The EDS analysis of the pitting

confirms the diffusion of the electrolyte and the dissolution of the protective layer in the corroded area, leaving exposed the substrate. The nitrided steel 1045 presents generalized corrosion, according to Figure 7d) in which it is observed the presence of a large number of holes in the surface, indicative that the nitrided steel 1045 is susceptible to severe corrosion.

4. Conclusion

Nanolayers composed of a mixture of nitrides were developed through short time and relatively low temperatures (500 °C and 550 °C) plasma nitriding process on hard chromium coated AISI 1045 steel. The Rietveld refinement of the nitrided samples 0.5° GIXRD patterns confirms the fact that nitrided layers are composed of a mixture of CrN, Cr₂N, Cr and Fe₄N. It also shows that higher nitrogen flows and a higher nitriding temperature promote greater

selectivity towards the CrN phase. Increasing the temperature amplifies the potential for nitriding, developing nanolayers of chromium nitride of approximately 500 nm. The obtained Chromium nitride nanolayers showed better corrosion resistance compared to hard chromium coated 1045 steel and nitrided steel. Nitrided samples showed more positive values of corrosion potentials, as well as corrosion current densities 10 times lower than base material, with a protective efficiency value of up to 90% in an H₂SO₄ electrolyte. The improvement in corrosion resistance could be attributed to the sealing of microcracks in the hard chromium layer and to the formation of a homogeneous nanolayer of fine-grained chromium nitrides within the area near the samples surface. These effects achieve without the need to use high temperatures and long periods nitriding times. These results confirm that the ceramic nanolayers of chromium nitrides developed at low temperatures and relatively short times by means of conventional ionic nitriding, could be potentialized for different technological applications, such as the development of bipolar plates or diluting magnetic semiconductors.

5. Acknowledgments

This work was financially supported by Tecnológico Nacional de México (grant 7779.20-P)

6. References

- Ranjbar K, Sababi M. Failure assessment of the hard chrome coated rotors in the downhole drilling motors. *Eng Fail Anal.* 2012;20:147-55. <http://dx.doi.org/10.1016/j.engfailanal.2011.11.007>.
- Menthe E, Rie K-T. Plasma nitriding and plasma nitrocarburizing of electroplated hard chromium to increase the wear and the corrosion properties. *Surf Coat Tech.* 1999;112:217-20. [http://dx.doi.org/10.1016/S0257-8972\(98\)00793-2](http://dx.doi.org/10.1016/S0257-8972(98)00793-2).
- Yu Y, Shironita S, Nakatsuyama K, Souma K, Umeda M. Surface composition effect of nitriding Ni-free stainless steel as bipolar plate of polymer electrolyte fuel cell. *Appl Surf Sci.* 2016;388:234-8. <http://dx.doi.org/10.1016/j.apsusc.2016.01.174>.
- Lee SH, Yang TH, Hyun SH, Yoon YS. Corrosion behavior of pre-oxidized and thermally nitrided stainless steel for polymer electrolyte membrane fuel cell bipolar plates. *Corros Sci.* 2012;58:79-85. <http://dx.doi.org/10.1016/j.corsci.2012.01.014>.
- Wang H, Brady MP, More KL, Meyer HM 3rd, Turner JA. Thermally nitrided stainless steels for polymer electrolyte membrane fuel cell bipolar plates Part 2: beneficial modification of passive layer on AISI446. *J Power Sources.* 2004;138:79-85. <http://dx.doi.org/10.1016/j.jpowsour.2004.06.064>.
- Brady MP, Wang H, Turner JA, Meyer HM 3rd, More KL, Tortorelli PF, et al. Pre-oxidized and nitrided stainless steel alloy foil for proton exchange membrane fuel cell bipolar plates: Part 1. Corrosion, interfacial contact resistance, and surface structure. *J Power Sources.* 2010;195:5610-8. <http://dx.doi.org/10.1016/j.jpowsour.2010.03.055>.
- Araujo JA, Souza RM, Batista de Lima N, Tschiptschin AP. Thick CrN/NbN multilayer coating deposited by cathodic arc technique. *Mater Res.* 2017;20(1):200-9. <http://dx.doi.org/10.1590/1980-5373-MR-2016-0293>.
- Gilewicz A, Chmielewska P, Murzynski D, Dobruchowska E, Warcholinski B. Corrosion resistance of CrN and CrCN/CrN Coatings deposited using cathodic arc evaporation in Ringer's and Hank's solutions. *Surf Coat Tech.* 2016;299:7-14. <http://dx.doi.org/10.1016/j.surfcoat.2016.04.069>.
- Monica CRG, de Castilho BCNM, Cunha C, Correr WR, Mordente P, Alvarez F, et al. On the effect of aluminum on the microstructure and mechanical properties of CrN coatings deposited by HiPIMS. *Mater Res.* 2018;21(3):1-6. <http://dx.doi.org/10.1590/1980-5373-MR-2017-0848>.
- Lavigne O, Alemany-Dumont C, Normand B, Berthon-Fabry S, Metkemeijer R. Thin chromium nitride PVD coatings on stainless steel for conductive component as bipolar plates of PEM fuel cells: ex-situ and in-situ performances evaluation. *Int J Hydrogen Energy.* 2012;37:10789-97. <http://dx.doi.org/10.1016/j.ijhydene.2012.04.035>.
- Han Z, Tian J, Lai Q, Yu X, Li G. Effect of N₂ partial pressure on the microstructure and mechanical properties of magnetron sputtered CrN_x films. *Surf Coat Tech.* 2003;162:189-93. [http://dx.doi.org/10.1016/S0257-8972\(02\)00667-9](http://dx.doi.org/10.1016/S0257-8972(02)00667-9).
- Hu YQ, Chen F, Xiang ZD. Cr₂N coated martensitic stainless steels by pack cementation process as materials for bipolar plates of proton exchange membrane fuel cells. *J Power Sources.* 2019;414:167-73. <http://dx.doi.org/10.1016/j.jpowsour.2019.01.002>.
- Dasgupta A, Kuppusami P, Vijayalakshmi M, Raghunathan VS. Pulsed plasma nitriding of large components and coupons of chrome plated SS316LN stainless steel. *J Mater Sci.* 2007;42(20):8447-53. <http://dx.doi.org/10.1007/s10853-007-1783-7>.
- Umm-i-kaloom, Ahmad R, Nisar A, Khan IA, Sehrish S, Uzma U, Nasarullah K. Effect of power and nitrogen content on the deposition of CrN films by using pulsed DC magnetron sputtering plasma. *Plasma Sci Technol.* 2013;15:666-72. <http://dx.doi.org/10.1088/1009-0630/15/7/12>.
- Romero J, Esteve J, Lousa A. Period dependence of hardness and microstructure on nanometric Cr/CrN multilayers. *Surf Coat Tech.* 2004;188-189:338-43. <http://dx.doi.org/10.1016/j.surfcoat.2004.08.058>.
- Guan X, Wang Y, Xue Q. Effects of constituent layers and interfaces on the mechanical and tribological properties of metal (Cr, Zr)/ceramic (CrN, ZrN) multilayer systems. *Appl Surf Sci.* 2020;502:144305. <http://dx.doi.org/10.1016/j.apsusc.2019.144305>.
- Kapczinski MP, Gil C, Kinast EJ, Alberto dos Santos C. Surface modification of titanium by Plasma Nitriding. *Mater Res.* 2003;2(6):265-71.
- Faga MG, Settineri L. Innovative anti-wear coatings on cutting tools for wood machining. *Surf Coat Tech.* 2006;201(6):3002-7. <http://dx.doi.org/10.1016/j.surfcoat.2006.06.013>.
- Wierzchon T, Ulbin-Pokorska I, Sikorski K. Corrosion resistance of chromium nitride and oxynitride layers produced under glow discharge conditions. *Surf Coat Tech.* 2000;130:274-9. [http://dx.doi.org/10.1016/S0257-8972\(00\)00696-4](http://dx.doi.org/10.1016/S0257-8972(00)00696-4).
- Sarraf SH, Soltanieh M, Aghajani H. Repairing the cracks network of hard chromium electroplated layers using plasma nitriding technique. *Vacuum.* 2016;127:1-9. <http://dx.doi.org/10.1016/j.vacuum.2016.02.001>.
- Aghajani H, Soltanieh M, Mahboubi F, Rastegari S, Nekouee KA. Formation of a hybrid coating by the use of plasma nitriding and hard chromium electroplating on the surface of H11 hot work tool steel. *Iranian Journal of Materials Science & Engineering.* 2009;6:31-7.
- Taktak S, Gunes I, Ulker S, Yalcin Y. Effect of N₂ + H₂ gas mixtures in plasma nitriding on tribological properties of duplex surface treated steels. *Mater Charact.* 2008;59:1784-91. <http://dx.doi.org/10.1016/j.matchar.2008.04.010>.
- Evangelina DLH, Ybarra G, Lamas D, Cabo A, Dalibon EL, Brühl SP. Plasma nitriding of 316L stainless steel in two different N₂-H₂ atmospheres - Influence on microstructure and corrosion resistance. *Surf Coat Tech.* 2017;313:47-54. <http://dx.doi.org/10.1016/j.surfcoat.2017.01.037>.

24. Wang L, Kim DS, Nam KS, Kim M, Kwon SC. Microstructure of electroplated hard chromium coatings after plasma nitrocarburizing. *Surf Coat Tech.* 2005;190:151-4. <http://dx.doi.org/10.1016/j.surfcoat.2004.08.213>.
25. Ajikumar PK, Sankaran A, Kamruddin M, Nithya R, Shankar P, Dash S, et al. Morphology and growth aspects of Cr(N) phases on gas nitridation of electroplated chromium on AISI 316 LN stainless steel. *Surf Coat Tech.* 2006;201:102-7. <http://dx.doi.org/10.1016/j.surfcoat.2005.10.043>.
26. Buijnsters JG, Shankar P, Sietsma J, ter Meulen JJ. Gas nitriding of chromium in NH₃/H₂ atmosphere. *Mater Sci Eng.* 2003;341:289-95. [http://dx.doi.org/10.1016/S0921-5093\(02\)00231-9](http://dx.doi.org/10.1016/S0921-5093(02)00231-9).
27. Rebholz C, Ziegele H, Leyland A, Matthews A. Structure mechanical and tribological properties of nitrogen-containing chromium coatings prepared by reactive magnetron sputtering. *Surf Coat Tech.* 1999;115:222-9. [http://dx.doi.org/10.1016/S0257-8972\(99\)00240-6](http://dx.doi.org/10.1016/S0257-8972(99)00240-6).
28. Wang L, Nam KS, Kwon SC. Effect of plasma nitriding of electroplated chromium coatings on the corrosion protection C45 mild steel. *Surf Coat Tech.* 2007;202:203-7. <http://dx.doi.org/10.1016/j.surfcoat.2007.05.027>.
29. Zhang GA, Yan PX, Wang P, Chen YM, Zhang JY. Influence of nitrogen content on the structure, electrical and mechanical properties of CrN_x thin films. *Mater Sci Eng.: A.* 2007;A460-461:301-5. <https://doi.org/10.1016/j.msea.2007.01.149>.
30. Taguchi M, Kurihara J. Effect of surface nitriding on corrosion resistance of chromium in sulfuric acid solution. *Mater Trans.* 1991;55(2):204-10. http://dx.doi.org/10.2320/jinstmet1952.55.2_204.
31. Dinu M, Mouele ESM, Parau AC, Vladescu A, Petrik LF, Braic M. Enhancement of the corrosion resistance of 304 stainless steel by Cr-N and Cr (N, O) coatings. *Coating.* 2018;8:2-10. <http://dx.doi.org/10.3390/coatings8040132>.
32. Wang D, Hu M, Jiang D, Fu Y, Wang Q, Sun JYJ, Weng L. The improved corrosion resistance of sputtered CrN thin films with Cr-ion bombardment layer by layer. *Vacuum.* 2017;143:329-35. <http://dx.doi.org/10.1016/j.vacuum.2017.06.040>.
33. Lang F, Yu Z. The corrosion resistance and wear resistance of thick TiN coatings deposited by arc ion plating. *Surf Coat Tech.* 2001;145:80-7. [http://dx.doi.org/10.1016/S0257-8972\(01\)01284-1](http://dx.doi.org/10.1016/S0257-8972(01)01284-1).